



TITLE:

# Unidirectional Spaser in Symmetry-Broken Plasmonic Core-Shell Nanocavity

AUTHOR(S):

Meng, Xiangeng; Guler, Urcan; Kildishev, Alexander V.; Fujita, Koji; Tanaka, Katsuhisa; Shalaev, Vladimir M.

---

CITATION:

Meng, Xiangeng ...[et al]. Unidirectional Spaser in Symmetry-Broken Plasmonic Core-Shell Nanocavity. Scientific Reports 2013, 3: 1241.

ISSUE DATE:

2013-02-07

URL:

<http://hdl.handle.net/2433/194142>

RIGHT:

This work is licensed under a Creative Commons Attribution-NonCommercial-NoDerivs 3.0 Unported License.



SUBJECT AREAS:

SOLID-STATE LASERS

NANOPHOTONICS AND  
PLASMONICS

NANOPARTICLES

NANOCAVITIES

Received  
30 October 2012

Accepted  
10 January 2013

Published  
7 February 2013

Correspondence and  
requests for materials  
should be addressed to  
X.G.M. (meng14@  
purdue.edu) or V.M.S.  
(shalaev@purdue.edu)

\* These authors  
contributed equally to  
this work.

# Unidirectional Spaser in Symmetry-Broken Plasmonic Core-Shell Nanocavity

Xiangeng Meng<sup>1,2\*</sup>, Urcan Guler<sup>1\*</sup>, Alexander V. Kildishev<sup>1</sup>, Koji Fujita<sup>2</sup>, Katsuhisa Tanaka<sup>2</sup> & Vladimir M. Shalaev<sup>1</sup>

<sup>1</sup>School of Electrical & Computer Engineering and Birck Nanotechnology Center, Purdue University, West Lafayette, IN 47907, USA, <sup>2</sup>Department of Material Chemistry, Graduate School of Engineering, Kyoto University, Katsura, Nishikyo-ku 615-8510, Kyoto, Japan.

The spaser, a quantum amplifier of surface plasmons by stimulated emission of radiation, is recognized as a coherent light source capable of confining optical fields at subwavelength scale. The control over the directionality of spasing has not been addressed so far, especially for a single-particle spasing nanocavity where optical feedback is solely provided by a plasmon resonance. In this work we numerically examine an asymmetric spaser – a resonant system comprising a dielectric core capped by a metal semishell. The proposed spaser emits unidirectionally along the axis of the semishell; this directionality depends neither on the incident polarization nor on the incident angle of the pump. The spasing efficiency of the semishell-capped resonator is one order of magnitude higher than that in the closed core-shell counterpart. Our calculations indicate that symmetry breaking can serve as a route to create unidirectional, highly intense, single-particle, coherent light sources at subwavelength scale.

The control over the directionality of emitted light in a conventional laser is usually accomplished through well-defined Fabry-Perot (FP) cavities composed of high-quality optical mirrors<sup>1</sup>. When an optical cavity is scaled down to the micrometer scale using a specific design, the system itself provides optical feedback without any external cavity. Depending on the geometric shape of the cavity and the dominant mode, laser emission from such a resonator can be either directional or omnidirectional. For instance, a single-nanowire laser emits longitudinally due to the FP cavity formed by the two parallel end faces<sup>2</sup>, while a circular microdisk resonator intends to emit isotropically because of its axial symmetry<sup>3</sup>. A plasmonic nanocavity can be scaled down to subwavelength dimensions due to its unique feedback mechanism<sup>4–23</sup>. Specific cavity designs such as FP cavities can be still employed to control the directionality of spaser emission for spasers based on the amplification of propagating surface plasmon polaritons, but particular challenges could arise when it comes to controlling the directionality of spaser emission achieved by the amplification of localized surface plasmons (LSPs) supported by a subwavelength-scale nanoparticle.

In this letter, we report on a single-particle spaser design with well-defined and unidirectional stimulated emission and highly effective laser output. By using a semishell-capped system design, we show that the laser emission can be guided and improved over previous spaser designs based on full-shell spasing nanocavity. The optical extinction properties of the semishell resonator (referred to as SSR) strongly depend on the incidence angle; nevertheless, spaser emission exclusively propagates along a specific direction. The power flow from the SSR is one order of magnitude higher than that from its full-shell resonator counterpart (referred to as FSR). This result opens up a new avenue for applications of high-intensity nanolasers. This approach allows for the integration of various gain materials, such as organic dyes, rare-earth nanocrystals, and semiconductor structures, within the nanolaser design. Thus, the proposed design is more compatible with semiconductor photonics and can be applied to fabricate lab-on-a-chip photonic circuits.

## Results

Our system consists of an optically active, spherical dielectric particle covered with a 10-nm-thick silver semishell (Fig. 1). The dispersion relationship of silver is described by the Drude-Lorentz model with five Lorentz oscillators<sup>24</sup>. The material of the core is chosen to be silica doped with optical gain inclusions (e.g., organic dyes, rare

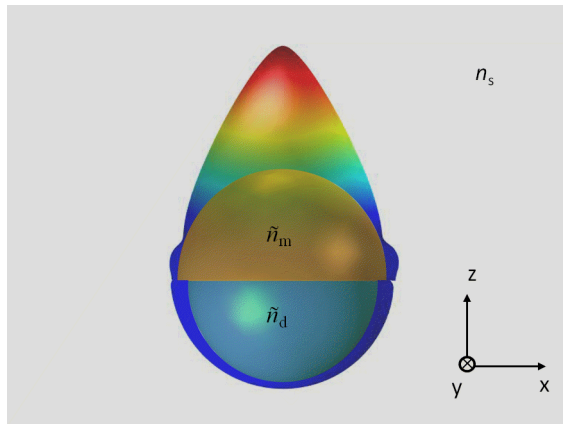


**Figure 1 | Light radiation from a metal semishell-capped spaser nanocavity.** The silver shell generates LSPs; the core provides optical gain to compensate for plasmon losses. Here the core is assumed to be silica doped with an optical gain material with refractive index  $\tilde{n}_d = 1.52 + i\kappa$ ,  $\kappa = -0.062$  for this image. The radius of the core is  $R = 100$  nm, and the shell thickness is  $t = 10$  nm. Spaser emission (colored beam) is unidirectional along the axis of the semishell as shown.

earth ions). Such materials can be fabricated through chemical covalent-bonding methods. We set the refractive index of the core to be constant (non-dispersive), i.e.,  $\tilde{n}_d = 1.52 + i\kappa$ , where the real part represents the refractive index of silica and  $\kappa$  defines the level of optical gain. The surrounding medium is air ( $n_s = 1$ ).

Optical extinction properties of the SSR strongly depend on the incident angle  $\theta_{\text{inc}}$  and are distinct from those of an FSR under the same  $p$ -polarized monochromatic illumination (Fig. 2a). This anisotropy is naturally expected in a nanostructure with broken symmetry. Resonance peaks observed for the case of SSR are very similar to the case of a bare metal semi-shell in air, except for the spectral shifts introduced by presence of the core. Thus, we can conclude that the extinction peaks are due to plasmon resonances of the metal shell. In this study, the plasmon mode centered at  $\lambda_{\text{res}} = 549$  nm is of particular interest; its optical extinction intensity is sensitive to  $\theta_{\text{inc}}$  and becomes more intense than the other modes under a certain  $\theta_{\text{inc}}$  (specifically, at  $\theta_{\text{inc}} = 90^\circ$ , as shown in Fig. 2a). The narrow linewidth confirms the mode's high  $Q$  factor of 23.9. This mode supports a mode volume  $V = 0.00042(\lambda/n)^3$ , where  $n$  is the refractive index of the core ( $n = 1.52$ ). The high  $Q$  factor and the deeply subwavelength-scale  $V$  give rise to a high Purcell factor  $F = 4326$ . Thus, as we expect, this mode should experience lower losses and is essential to achieving low-threshold surface plasmon (SP) amplification. Hence we focus at this particular mode for the rest of our study.

Figure 2b shows the evolution of absorption and scattering cross sections (denoted by  $\sigma_{\text{abs}}$  and  $\sigma_{\text{sca}}$ ) with  $\kappa$  ranging from 0 to  $-0.21$  under  $\theta_{\text{inc}} = 0^\circ$ . The magnitudes of  $\sigma_{\text{abs}}$  and  $\sigma_{\text{sca}}$  increase rapidly when  $\kappa$  decreases from 0 to  $-0.062$ , the magnitudes decline when  $\kappa$

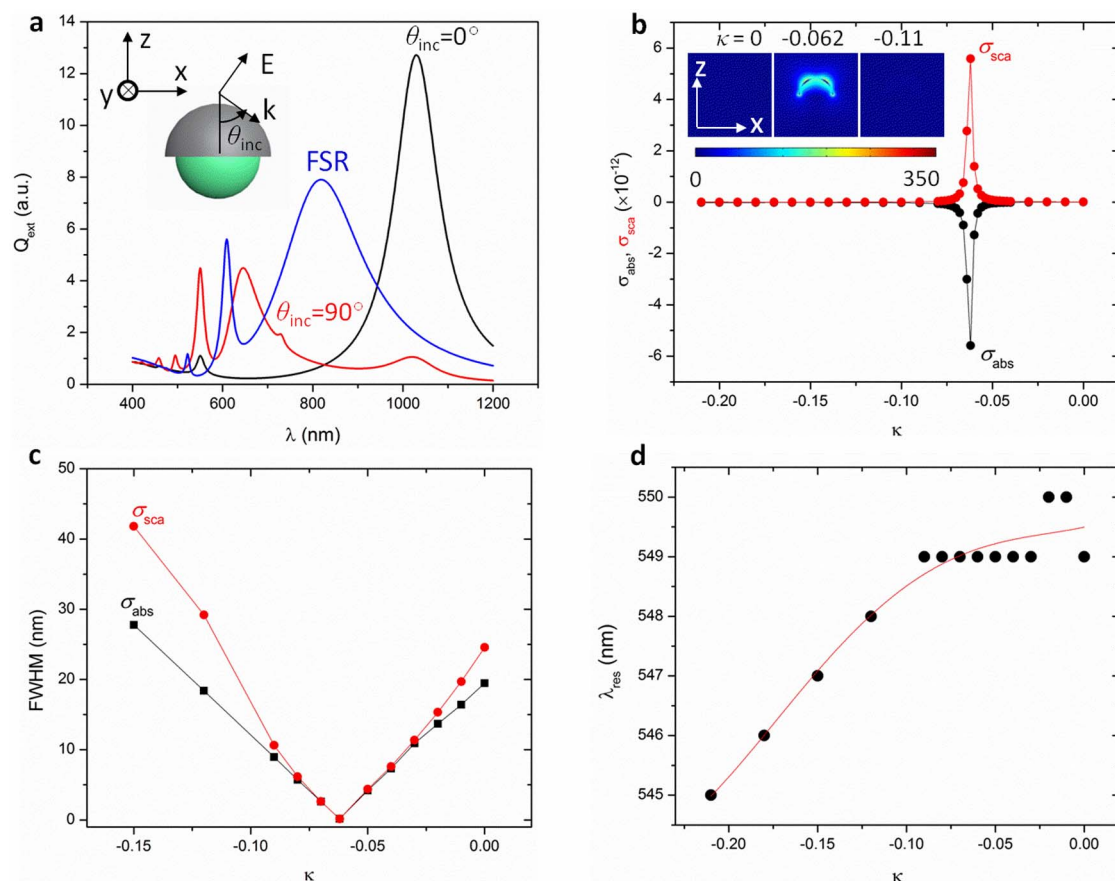


**Figure 2 | Optical extinction properties of SSR.** (a), Optical extinction spectra under  $\theta_{\text{inc}} = 0$  (black line, light propagates along  $z$  direction) and  $90^\circ$  (red line, light propagates along  $x$  direction) for an SSR with  $\kappa = 0$ . The inset shows the excitation configuration. The optical extinction of an FSR is included for comparison (blue line). (b–d),  $\kappa$ -dependence of  $\sigma_{\text{abs}}$  ( $\sigma_{\text{sca}}$ ), FWHM, and  $\lambda_{\text{res}}$ . The insets in (b) presents the electric field distribution in the ( $x$ – $z$ ) plane at  $\kappa = 0$ ,  $-0.062$ , and  $-0.11$ , respectively. The discrete data in (b–d) represent the simulation results, and the solid lines are used to guide the observation.

$< -0.062$ , and  $\sigma_{\text{abs}}$  becomes negative when  $\kappa < -0.02$ . The existence of an optimal  $\kappa$  in FSR-based systems has been already shown previously<sup>25</sup>. The underlying mechanism is related to the dynamics of spasers: the maximum spasing efficiency is achieved at a zero-level net optical gain<sup>16</sup>. The optical extinction cross section ( $\sigma_{\text{ext}}$ ), i.e., the sum of  $\sigma_{\text{abs}}$  and  $\sigma_{\text{sca}}$ , is close to zero at  $\kappa \sim -0.062$ .  $\sigma_{\text{ext}}$  is positively maximum when  $\kappa$  is slightly larger than  $-0.062$ , while negatively maximum when  $\kappa$  is slightly smaller than  $-0.062$ . Thus, the value of  $\kappa \sim -0.062$  can be viewed as the threshold for spasing, which gives rise to the highest magnitude of  $\sigma_{\text{abs}}$  and  $\sigma_{\text{sca}}$ . The optimal  $\kappa$  value decreases with the increase of  $n_s$  (Fig. S1). Spectral narrowing occurs for both absorption and scattering when  $\kappa < 0$  (Fig. 2c). The full width of half maximum (FWHM) of the absorption spectrum is  $\sim 19.5$  nm at  $\kappa = 0$ , it narrows down to  $0.15$  nm at  $\kappa = -0.062$ , and then it widens again when  $\kappa < -0.062$ . The spectral narrowing and the occurrence of the negative  $\sigma_{\text{ext}}$  indicate that the level of optical gain is sufficient to compensate for plasmon losses, and thus spasing occurs. The giant enhancement of the local electric field (inset of Fig. 2b) serves as additional evidence for spasing. When the  $\kappa$  value changes, the value of  $\lambda_{\text{res}}$  shifts only slightly (Fig. 2d).

A systematic study on the  $\theta_{\text{inc}}$ -dependent optical properties of an SSR is depicted in Fig. 3a. The maximum  $\sigma_{\text{abs}}$  and  $\sigma_{\text{sca}}$  appear at  $\theta_{\text{inc}} = 90^\circ$  and are more than eight times higher than those at  $\theta_{\text{inc}} = 0^\circ$ . The optimal performance at  $\theta_{\text{inc}} = 90^\circ$  is related to the high local fields under this  $\theta_{\text{inc}}$  (Fig. S2), which confines light more tightly and thus provides more intense optical feedback for SP amplification. The values of  $\sigma_{\text{abs}}$  and  $\sigma_{\text{sca}}$  achieved in an SSR for  $\kappa = -0.062$  and  $\theta_{\text{inc}} = 90^\circ$  are  $\sim 745$  times higher than those at  $\kappa = 0$ , and  $\sim 6$  times higher than that achieved in an FSR ( $\lambda_{\text{res}} = 608$  nm) with the same gain level (Fig. S3).

The intensities of the near- and far-field electric field patterns are also sensitive to  $\theta_{\text{inc}}$  (Figs. 3b and 3c). The angular patterns for near and far fields, given in Fig. 3b–c, are different from each other, as can be expected from an analogy to a dipole emitter. Similar to optical cross sections, a maximum magnitude of near- and far-field intensity is achieved at  $\theta_{\text{inc}} = 90^\circ$ . Of particular interest is that the power flow from an SSR is unidirectional and independent of  $\theta_{\text{inc}}$ , although its magnitude varies with  $\theta_{\text{inc}}$  and reaches a maximum at  $\theta_{\text{inc}} = 90^\circ$  (Fig. 3d). The pattern of the power flow in the presence of optical gain ( $\kappa = -0.062$ ) is distinct from that of the passive SSR ( $\kappa = 0$ , Fig. S4). However, the scattered component is similar between the active ( $\kappa = -0.062$ ) and passive ( $\kappa = 0$ ) systems. This provides direct evidence that the lasing in an SSR arises from the amplification of SPs scattered backwards, and this in turn forms the basis of the directionality of the spaser emission since the scattering component of SSR with  $\kappa = 0$  unidirectionally propagates in the same direction with spaser emission. The magnitude of the power flow from the SSR with  $\kappa = -0.062$  is one order of magnitude higher than that from an FSR at  $\theta_{\text{inc}} = 90^\circ$  (Fig. S4) with the same  $\kappa$  value. The directional lasing and high efficiency are essential for a direct probe of single-particle lasing and for practical applications. Our further simulations show that the directionality appears for *s*-polarized illumination as well (Fig. S5), indicating that the directionality is independent of the incident polarization.

## Discussion

Symmetry breaking can bring significant advantages to plasmonics, which can be related to the appearance of new plasmon modes

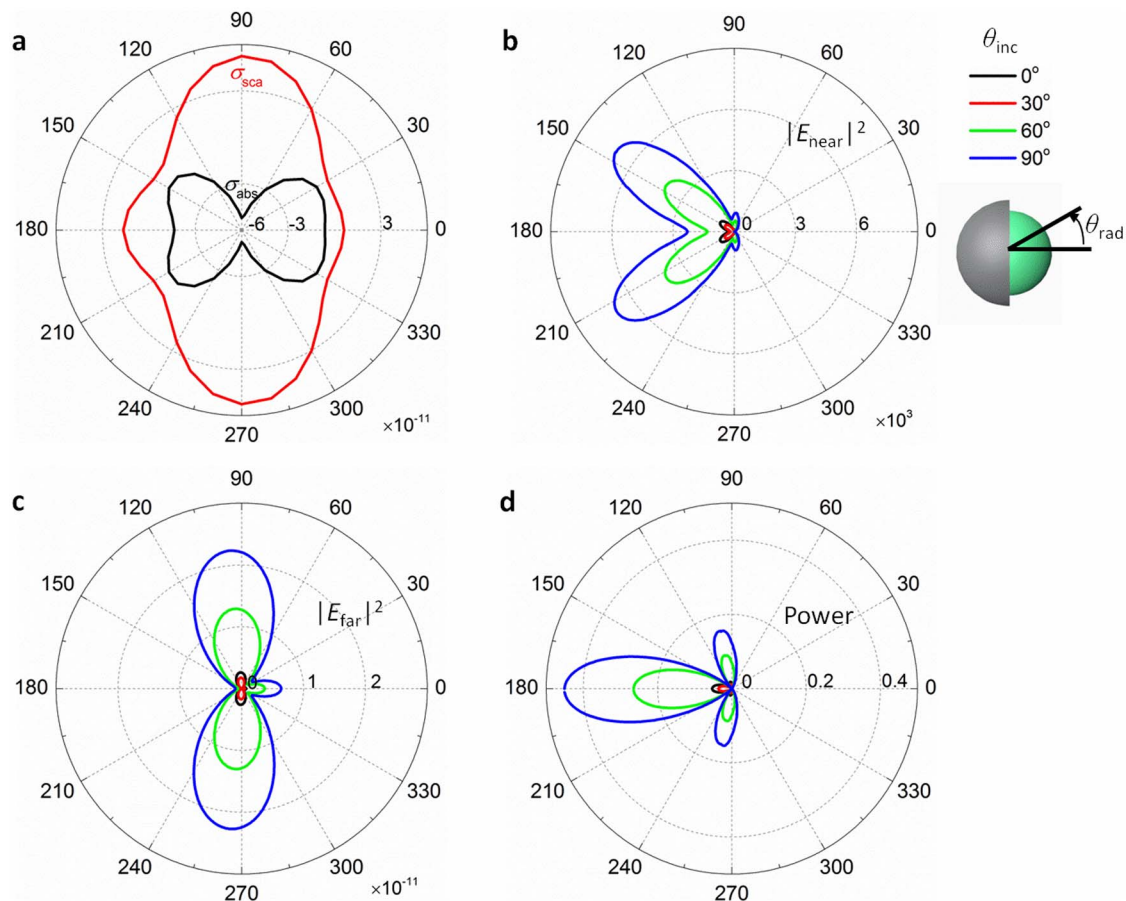


**Figure 3 | Polarization-sensitive optical properties of an SSR.** (a),  $\theta_{\text{inc}}$ -dependent  $\sigma_{\text{abs}}$  (black line) and  $\sigma_{\text{sca}}$  (red line). (b–d), Polar plots of the intensities of near-field electric field (b), far-field electric field (c), and power flow patterns at various  $\theta_{\text{inc}}$ . The legend is for (b–d), indicating the values of  $\theta_{\text{inc}}$ . The value of  $\kappa$  is  $-0.062$  for all the plots. The angle of radiation ( $\theta_{\text{rad}}$ ) is defined in the right.



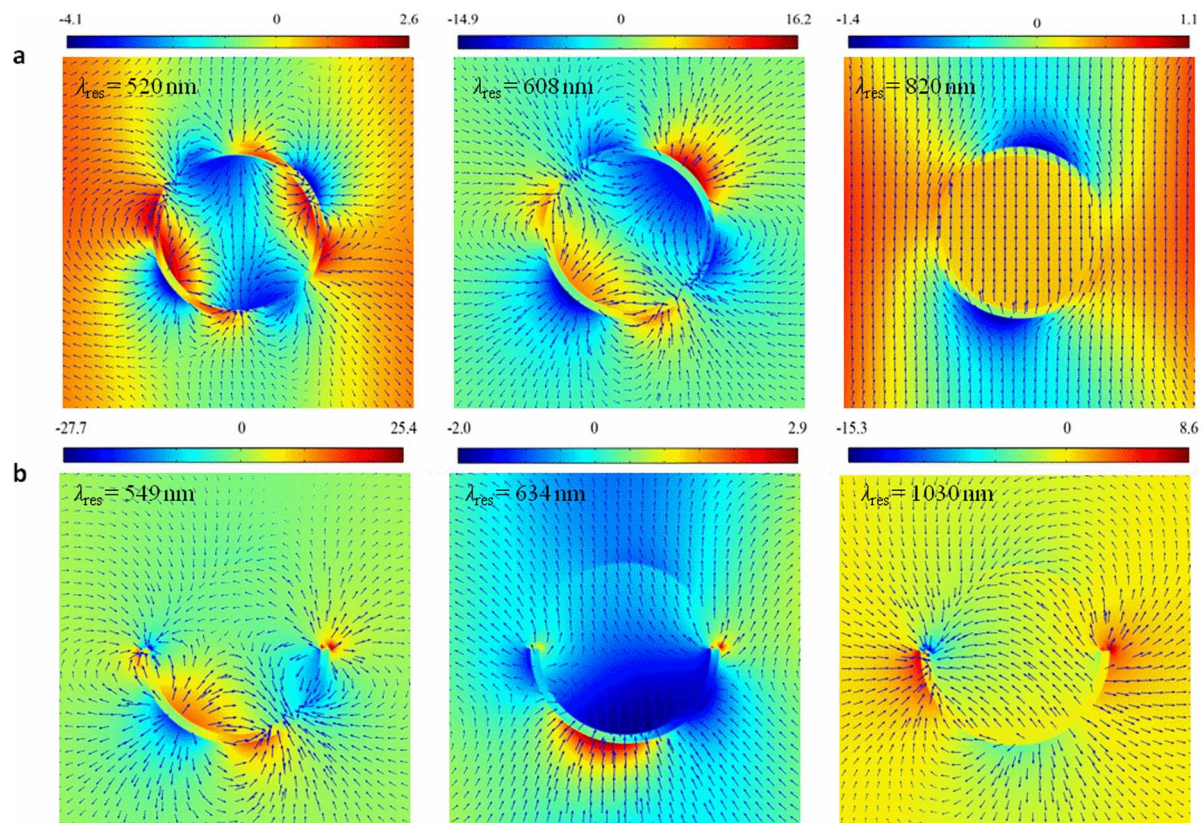


**Figure 4 | Evolution of plasmon modes when an FSR is reduced to an SSR.** (a), plasmon modes in an FSR:  $\lambda_{\text{res}} = 520$  nm, hexapole mode;  $\lambda_{\text{res}} = 608$  nm, quadrupole mode; and  $\lambda_{\text{res}} = 820$  nm, dipole mode. (b), plasmon modes in an SSR:  $\lambda_{\text{res}} = 549$  nm, quadrupole mode;  $\lambda_{\text{res}} = 634$  nm, dipole mode (axial)<sup>27</sup>; and  $\lambda_{\text{res}} = 1030$  nm, dipole mode (transverse)<sup>27</sup>. Field maps show the total field while arrows show the scattered components.

induced by the broken symmetry, as has been reported in C-shaped optical antennas<sup>26</sup>. Both of the lasing modes in an SSR ( $\lambda_{\text{res}} = 549$  nm) and FSR ( $\lambda_{\text{res}} = 608$  nm) can be assigned to a quadrupole oscillation, as clearly shown in Fig. 4. The combination of higher local field intensities and a lower metal content in an SSR naturally reduces the dissipative losses from the metal and thus leads to higher efficiency for nanolaser emission. The nature of other plasmon modes in either an FSR or an SSR can be assigned as well (Fig. 4). For completeness, we have also analyzed the optical properties of the other modes in the SSR structure, but none of them can offer directional lasing (Fig. S6.1–S6.4). The magnitudes of the fields in the near field and in the far field, as well as the power flow, are much lower than those achieved through the octupole mode.

In terms of experimental feasibility, an SSR clearly outperforms an FSR. The FSR core-shell nanoparticles are typically produced via a chemical procedure and require stringent fabrication<sup>8</sup>; in contrast, SSRs can be fabricated by physically depositing a thin layer of metal on an array of dielectric gain particles<sup>27</sup>. This allows for a versatile selection of optical gain materials as well as the species of the metal. Although the 10 nm-thick silver layer chosen here is quite thin, it can be manufactured effectively by adopting a specific fabrication technique that can make the semishell layer ultra-smooth and continuous<sup>28</sup>.

To conclude, we have proposed an approach based on symmetry breaking to create unidirectional nanolasers in a single-particle spasing nanocavity. This approach provides power flows that are one order of magnitude higher than those in the closed-resonator counterpart, which is essential to build high-intensity and subwavelength-scale nanolaser sources for practical applications. In addition to nanolaser applications, this structure holds potential for single-molecule probes owing to the enormously enhanced light scattering by the optical gain in the system.

## Methods

**Simulation.** Calculations were performed with a commercial software package (COMSOL, Multiphysics) based on the finite element method (FEM) in the frequency domain. A scattered-field formalism was used, and half of the physical system was simulated because of the mirror symmetry relative to the incident plane. The wavelength and incidence angle of the monochromatic plane wave incident on the semi-shell system were each varied separately in the simulations. The 3D simulation domain consisted of the core and shell of the particle system, the host medium and a perfectly matched layer (PML).

Near-field angular data were calculated by normalizing the total field intensity with the incident light intensity. Far-field patterns were calculated from the near-field values via the Stratton-Chu formula<sup>29</sup>. Power flow values were obtained by using the radial component of the time-averaged Poynting vector at an external, virtual spherical surface that is concentric with the nanolaser system.

**Mode volume and Purcell factor.** The mode volume of the SSR was calculated using the formula

$$V = \frac{\int \epsilon(\vec{r}) |\vec{E}(\vec{r})|^2 d^3r}{\max[\epsilon(\vec{r}) |\vec{E}(\vec{r})|^2]}, \quad (1)$$

where  $\epsilon(\vec{r})$  is the dielectric constant at the position  $\vec{r}$ , and  $|\vec{E}(\vec{r})|^2$  is the corresponding field intensity<sup>17</sup>. Using the FEM software package, we calculated the field distribution for the SSR and then the mode volume using Eq. (1). The quality factor was estimated by  $Q = \lambda_{\text{res}}/\Delta\lambda$ , where  $\lambda_{\text{res}}$  is the resonant wavelength, and  $\Delta\lambda$  is the spectral linewidth. The Purcell factor was calculated from the formula.

$$F = \frac{3Q}{4\pi^2 V} \left( \frac{\lambda_{\text{res}}}{n} \right)^3. \quad (2)$$

1. Svelto, O. *Principles of Lasers* (Springer, 1998).
2. Johnson, J. C. *et al.* Single gallium nitride nanowire lasers. *Nature Mater.* **1**, 106–110 (2002).
3. Song, Q. H. *et al.* Directional laser emission from a wavelength-scale chaotic microcavity. *Phys. Rev. Lett.* **105**, 103902 (2010).
4. Bergman, D. J. & Stockman, M. I. Surface plasmon amplification by stimulated emission of radiation: quantum generation of coherent surface plasmons in nanosystems. *Phys. Rev. Lett.* **90**, 027402 (2003).

5. Seidel, J., Grafström, S. & Eng, L. Stimulated emission of surface plasmons at the interface between a silver film and an optically pumped dye solution. *Phys. Rev. Lett.* **94**, 177401 (2005).
6. Noginov, M. A. *et al.* Stimulated emission of surface plasmon polaritons. *Phys. Rev. Lett.* **101**, 226806 (2008).
7. Ambati, M. *et al.* Observation of stimulated emission of surface plasmon polaritons. *Nano Lett.* **8**, 3998–4001 (2008).
8. Wegner, M. *et al.* Toy model for plasmonic metamaterial resonances coupled to two-level system gain. *Opt. Exp.* **16**, 19785–19788 (2008).
9. Zheludev, N. I., Prosvirnin, S. L., Papasimakis, N. & Fedotov, V. A. Lasing spaser. *Nature Photon.* **2**, 351–354 (2008).
10. Noginov, M. A. *et al.* Demonstration of a spaser-based nanolaser. *Nature* **460**, 1110–1113 (2009).
11. Oulton, R. F. *et al.* Plasmonic lasers at deep subwavelength scale. *Nature* **461**, 629–632 (2009).
12. Gather, M. C., Meerholz, K., Danz, N. & Leosson, K. Net optical gain in a plasmonic waveguide embedded in a fluorescent polymer. *Nature Photon.* **4**, 457–461 (2010).
13. De Leon, I. & Berini, P. Amplification of long-range surface plasmons by a dipolar gain medium. *Nature Photon.* **4**, 382–387 (2010).
14. Xiao, S. *et al.* Loss-free and active optical negative-index metamaterials. *Nature* **466**, 735–738 (2010).
15. Stockman, M. I. Spaser action, loss compensation, and stability in plasmonic systems with gain. *Phys. Rev. Lett.* **106**, 156802 (2011).
16. Stockman, M. I. The spaser as a nanoscale quantum generator and ultrafast amplifier. *J. Opt.* **12**, 024004 (2010).
17. Hill, M. T. *et al.* Lasing in metallic-coated nanocavities. *Nature Photon.* **1**, 589–594 (2007).
18. Nezhad, M. P. *et al.* Room-temperature subwavelength metallo-dielectric lasers. *Nature Photon.* **4**, 395–399 (2010).
19. Ma, R. M., Oulton, R. F., Sorger, V. J., Bartal, G. & Zhang, X. Room-temperature sub-diffraction-limited spaser by total internal reflection. *Nature Mater.* **10**, 110–113 (2011).
20. Khajavikhan, M. *et al.* Thresholdless nanoscale coaxial lasers. *Nature* **482**, 204–207 (2012).
21. Berini, P. & De Leon, I. Surface plasmon-polariton amplifiers and lasers. *Nature Photon.* **6**, 16–24 (2012).
22. Ding, K. *et al.* Room-temperature continuous wave lasing in deep-subwavelength metallic cavities under electric injection. *Phys. Rev. B* **85**, 041301 (2012).
23. Lu, Y. J. *et al.* Plasmonic nanolaser using epitaxially grown silver film. *Science* **337**, 450–453 (2012).
24. Ni, X., Liu, Z. & Kildishev, A. V. *PhotonicsDB: Optical constants* (2007).
25. Gordon, J. A. & Ziolkowski, R. W. The design and simulated performance of a coated nano-particle laser. *Opt. Express* **15**, 2622–2653 (2007).
26. Shi, X., Hesselink, L. & Thornton, R. L. Ultrahigh light transmission through a C-shaped nanoaperture. *Opt. Lett.* **28**, 1320–1322 (2003).
27. Mirin, N. A., Ali, T. A., Nordlander, P. & Halas, N. J. Perforated semishells: far-field directional control and optical frequency magnetic response. *ACS Nano* **5**, 2701–2712 (2010).
28. Chen, W., Thoreson, M. D., Ishii, S., Kildishev, A. V. & Shalae, V. Ultra-thin ultra-smooth and low-loss silver films on a germanium wetting layer. *Opt. Express* **18**, 5124–5134 (2010).
29. Stratton, J. *Electromagnetic Theory* (New York: McGraw-Hill, 1941).

## Acknowledgments

This work was supported in part by Air Force Office of Scientific Research Grant (FA9550-10-1-0264), National Science Foundation Grant (DMR-1120923), NSF “Meta-PREM” grant (1205457), and by grant in-Aid for Scientific Research B (24350104) and for Challenging Exploratory Research (24656385) from MEXT, Japan. XM thanks financial support from Young Researcher Overseas Visits Program for Vitalizing Brain Circulation of JSPS, Japan.

## Author contributions

X.M. conceived the concept, performed the simulation, and wrote the paper. U.G. performed the simulation and contributed to the manuscript preparation. A.V.K., K.F. and K.T. analyzed the data and contributed to the manuscript preparation. V.M.S. supervised the whole work. All authors read and corrected the manuscript before submission.

## Additional information

**Supplementary information** accompanies this paper at <http://www.nature.com/scientificreports>

**Competing financial interests:** The authors declare no competing financial interests.

**License:** This work is licensed under a Creative Commons Attribution-NonCommercial-NoDerivatives 3.0 Unported License. To view a copy of this license, visit <http://creativecommons.org/licenses/by-nc-nd/3.0/>

**How to cite this article:** Meng, X.G. *et al.* Unidirectional Spaser in Symmetry-Broken Plasmonic Core-Shell Nanocavity. *Sci. Rep.* **3**, 1241; DOI:10.1038/srep01241 (2013).